Tetrahedral calcite crystals facilitate self-assembly at the air-water interface

S. M. Hashmi
Division of Engineering and Applied Sciences, Harvard University, Cambridge, Massachusetts 02138, USA

H. H. Wickman
National Science Foundation, 4201 Wilson Boulevard, Arlington, Virginia 22230, USA

D. A. Weitz
Division of Engineering and Applied Sciences, Harvard University, Cambridge, Massachusetts 02138, USA and Department of Physics, Harvard University, Cambridge, Massachusetts 02138, USA

(Received 8 June 2005; published 26 October 2005)

Calcite crystals often nucleate and grow in solutions of calcium carbonate, and these crystallites can become trapped at the air water interface, where they form unusual structures. The most common is a fractal structure, which can extend over a large fraction of the interface, and whose origin is understood in terms of the aggregation of the particles. Much more rarely, a different and entirely unexpected structure is observed: the particles remain well separated on the interface, forming an ordered phase reminiscent of a two-dimensional colloidal crystal. The structure of the crystallites that form this ordered phase is always observed to be tetrahedral, in contrast to the much more common rhombohedral structure of the crystallites that form the fractal phase. We show that the interparticle interaction potential that leads to this ordered phase is a balance between a long-range attractive interaction and a long-range repulsive interaction. The attraction results from gravity-induced capillary forces, while the repulsion results from a dipole-dipole interaction due to the charged surface of the tetrahedral crystals. The interaction potential is estimated from the thermal motion of the particles, and fits to the theoretically expected values suggest that the effective surface charge on the tetrahedral crystals is $\sigma \sim 0.01$ charges/nm^2.

DOI: 10.1103/PhysRevE.72.041605 PACS number(s): 81.10.Dn, 82.70.Dd, 41.20.Cv, 68.43.Hn

INTRODUCTION

Calcium carbonate is an important biomineral whose crystal phases and structures, dissolution behaviors, and growth habits on various substrates have been studied extensively. Interesting structures are observed when calcium carbonate crystals are constrained at fluid interfaces. Calcium carbonate precipitating out of aqueous solution is known to form fractal aggregates of micron-sized rhombohedral calcite crystals on the air-water interface [1]. The formation of these fractal aggregates requires short-range attractive forces which cause individual particles to stick to each other. This short-range attraction arises from van der Waals forces. However, the aggregation is enhanced by a long-range attraction which also occurs for sufficiently large particles at a fluid interface. This is the capillary attraction, which requires a deformation of the interface [2,3]. This is the same sort of attraction which causes pieces of cereal to clump together at the surface of milk in a cereal bowl. A flat interface costs less energy than a curved one, so two particles deforming an interface in the same way will attract each other to lessen the surface deformation [2,4]. Calcite crystals of sufficient size cause a deformation of the interface through gravity. Calcite crystal aggregation is thus driven by capillary attraction at large separations and van der Waals forces near contact, in a process similar to diffusion-limited aggregation [1,3].

A distinct and unexpected phenomenon is observed to coexist with the aggregate: the ordering of calcite crystals on the interface. This phenomenon is observed when aqueous solution is heated before the calcite crystal growth occurs. Furthermore this ordered phase specifically requires crystals of tetrahedral morphology. Tetrahedral crystals are not the preferred morphology of calcite; instead rhombohedral crystals are preferred. Nevertheless tetrahedral crystals are observed to form when calcium carbonate is grown on monolayer films made of acidic organic polymers [5]. Though the ordering of tetrahedral crystals is uncommon, it is observed as a result of a modified Kitano crystallization process, in which a stirred supersaturated calcium bicarbonate solution is purged with carbon dioxide [6]. Wickman and Korley observe the ordering of tetrahedral calcite crystals at the air-water interface in samples made from aged aqueous solutions which had been heated before sample preparation; they name the ordering phenomenon the "*w* layer" [7].

The forces leading to the stability of the *w* layer are not well understood. Both attractive and repulsive interactions between particles are essential to cause the observed ordering. While the attraction may arise from capillary forces, the origin of the required repulsive force is unknown. Understanding this repulsive force is essential to a complete understanding of the behavior of the *w* layer.

In this paper we determine the conditions which lead to the formation of the *w* layer and analyze the behavior of the *w*-layer crystals to understand the repulsive forces involved in its formation. We observe the *w* layer through a microscope and investigate more closely individual crystallites that make up the *w* layer to determine their surface chemistry. We track the positions of the *w*-layer crystals over time and extract both the equilibrium separation distance between the crystals and the stiffness of their interparticle interaction. We

find that the behavior of the *w*-layer crystals is consistent with an interparticle interaction consisting of forces due to capillary attraction and an electrostatic repulsion mediated by the surface chemistry of the *w*-layer crystals themselves.

OBSERVATIONS AND DISCUSSION

We prepare aqueous solutions of calcium oxide at concentrations between 4 and 5 mM. Both fresh solutions and solutions up to 2 months old are used to make samples. Samples are made by combining 1 ml of solution with 1 ml triple-distilled, de-ionized water in a plastic Petri dish 3.5 cm in diameter. For most samples the solution is heated in a water bath to temperatures between 40 and 45 °C for approximately 5 min, and the sample is made immediately thereafter. For the remaining samples the solution is not heated before sample preparation. We visualize the sample with a Leica inverted microscope using 10× or 63× dry objectives. We image the sample using a Cohu high performance charge coupled device (CCD) camera and digitally record images and videos.

The sample is exposed to carbon dioxide from the air, allowing calcium carbonate crystals to precipitate and grow in the form of calcite. Near the beginning of the crystal formation process, small crystallites are sometimes seen to rise through the bulk of the sample to the surface of the water where they are trapped by surface tension. We also observe the growth of crystals at the surface, where they are entrained by surface tension. When the crystal formation process is complete, single crystals are found both at the bottom of the Petri dish and at the air-water interface. Final crystal sizes range from 5 to 30 μm across an edge. Samples made from fresh solutions yield significantly more crystal mass than those made from aged solutions.

Our observations show that crystals form while rising through the bulk of the sample, even though calcite is much denser than water. Therefore the crystals must become buoyant due to something else in the system. We speculate that the crystals may nucleate on bubbles of gas, gain buoyancy from them, and thus rise to the surface [8]. In order to explain the origin of the required gas bubbles, we suggest a multistep chemical reaction which can account for the precipitation of calcite. Prior to crystal formation, the *p*H level of the calcium oxide in solution is measured to be near 11, suggesting that calcium, a strong base, dissociates rather than remaining in solution as $Ca(OH)_2$:

$$CaO_{(s)} + H_2O \leftrightarrow Ca^{2+}_{(aq)} + 2(OH^-)_{(aq)}. \quad (1)$$

Carbon dioxide also dissolves in water

$$CO_{2(g)} + H_2O \rightarrow H^+_{(aq)} + HCO^-_{3(aq)}. \quad (2)$$

The carbonate ions produced from the dissolution of carbon dioxide can react with the calcium ions to produce calcium carbonate

$$Ca^{2+}_{(aq)} + 2HCO^-_{3(aq)} \rightarrow CaCO_3\downarrow + CO_2\uparrow + H_2O. \quad (3)$$

A similar process in which calcite crystals nucleate on escaping carbon dioxide has also been seen with the Kitano crystallization method [9]. The carbon dioxide thus provides buoyancy to the growing crystals, bringing them to the air-water interface. After crystallization, the *p*H of the sample is measured to be a neutral 7, consistent with the proposed reaction mechanism. However, both preheating the solution and cooling the sample may alter the evaporation rate as well as the solubilities of the compounds, possibly affecting the crystallization. Nevertheless, our proposed reaction scheme remains a plausible hypothesis for both the formation of the crystals and their appearance at the air-water interface.

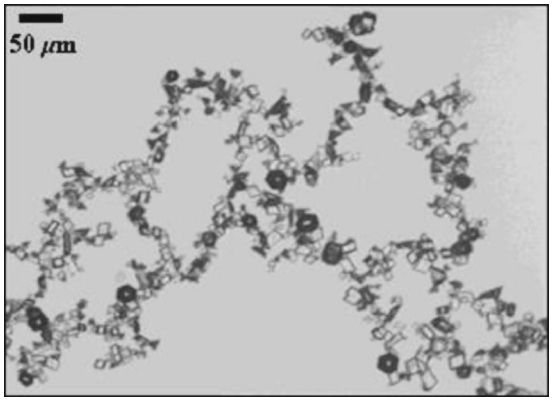

FIG. 1. An example of a fractal mat of calcium carbonate crystals at the air-water interface. The crystals possess many different morphologies.

Typically, cluster-cluster aggregation at the air-water interface produces a fractal mat structure within about an hour. The fractal mat is composed of crystals with various morphologies. The most common crystal morphology found in the fractal mat is rhombohedral. A typical section of the fractal mat is shown in Fig. 1. Growth of the fractal mat continues until every crystal on the interface is incorporated. Complete fractal mats may span areas as large as a few square centimeters. Agitation may dislodge pieces from each other, but those pieces will eventually reaggregate. The fractal mat is seen in every sample of calcite crystals at the air-water interface.

Surprisingly, calcite crystals may also arrange themselves into an ordered region on the interface, the *w* layer. The *w*-layer mass is generally less than 10% of the mass of fractal mat in a given sample. The *w* layer is seen in samples made from fresh and aged solutions alike. However, this phenomenon is observed only when the solution is heated before sample preparation. The ordering occurs before or at about the same time as the completion of the fractal mat. Some sections of *w* layer are confined on all sides by sections of the fractal mat, as shown in Fig. 2. However, the *w* layer also occupies unconstrained spaces on the periphery of the fractal mat, as shown in Fig. 3. The nearly perfect ordering of the *w* layer is hexagonal with fivefold and sevenfold defects, and is seen most clearly in Fig. 3. Sometimes a given crystal may have only four nearest neighbors.

The origin of the *w* layer must differ greatly from that of the fractal mat, as the fractal mat requires attractive forces alone. The existence of the *w* layer in an unconfined geometry requires that the interparticle potential between the *w*-layer crystals consist of both attractive and repulsive

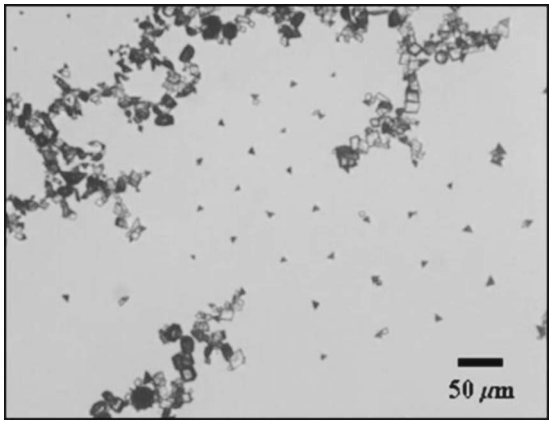

FIG. 2. A typical image of a constrained section of the *w* layer.

forces. Repulsive forces are sufficient to cause ordering in a system with a constrained area. However, the presence of the *w* layer in an unconstrained area suggests that a long-range attraction is indeed present as well. In other systems at the air-water interface, order has been known to arise from electrostatic forces, irregular meniscus effects, van der Waals forces, and capillary interactions [2,3,10,11]. Normally, calcite crystals experience attractive forces only, as evidenced by the ubiquitous nature of the fractal mat. These forces are due to capillary attraction which results from the distortion of the interface. The long-range attraction required to form the *w* layer may presumably be the same capillary attraction which forms the fractal mat.

The origin of the long-range repulsion required to form the *w* layer must be inferred from investigation of the *w* layer itself, since no repulsive forces are involved in the fractal mat. We find that single tetrahedral crystals usually occupy each site of the *w*-layer lattice, an example of which is shown in Fig. 4. However, some sites of the *w* layer may be occupied by a dimer or trimer consisting of one tetrahedron and one or two rhombohedra. A single rhombohedral crystal is never seen to occupy a position in the *w* layer on its own, nor is a dimer of two tetrahedral crystals. In fact, two tetrahedra do not generally aggregate together at all without a

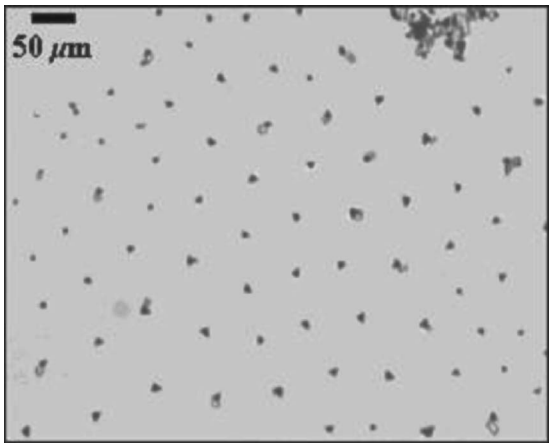

FIG. 3. A typical image of an unconstrained section of the *w* layer. The ordered phase exhibits nearly perfect hexagonal ordering.

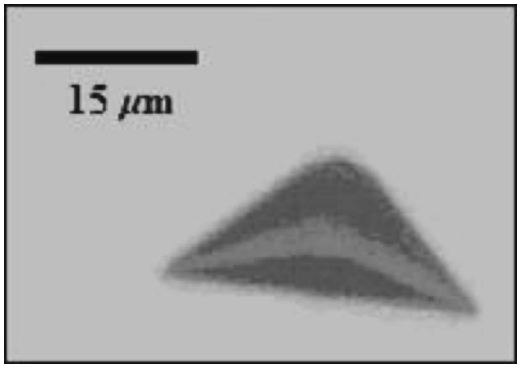

FIG. 4. A typical single tetrahedral crystal occupying a lattice site in the *w* layer.

few rhombohedral crystals between them. Typical tetrahedral crystal sizes range between 10 and 30 μm across the longest edge.

Tetrahedral crystals are not the preferred morphology of calcite and their crystal structure may explain why this relatively rare morphology dominates the *w* layer. The preferred morphology of calcite is a rhombohedral crystal with six faces, each nucleated on the crystal plane of calcite given by the Millar index (104) [12]. To understand the relation between tetrahedral and rhombohedral morphologies, we note that cleaving the corner of a rhombohedral calcite crystal would result in a tetrahedral crystal with three equivalent (104) faces and a fourth face on a different crystal plane. To test that the tetrahedral *w*-layer crystals similarly have three equivalent (104) faces, we observe individual tetrahedral crystals on a smaller scale in a scanning electron microscope (SEM). To prepare a sample for the SEM, a transmission electron microscope (TEM) grid is placed under the air-water interface and raised to remove the crystals. The TEM grid sample is left to fully air-dry and sputter-coated with a thin layer of gold for viewing in the SEM. A closer look at a tetrahedral crystal does suggest that the tetrahedral calcite crystals indeed have three equivalent (104) faces and a fourth face on a different plane. The three basal corners of this crystal were broken as this crystal was removed from the air-water interface for viewing in the SEM, as shown in Fig. 5; only the apex remains intact. The (104) plane must be expressed where the crystal has broken, as this is the natural cleavage plane of calcite [12]. The original faces of the crystal are parallel to the broken faces, suggesting that they also express the (104) plane of calcite.

The main difference between rhombohedral and tetrahedral calcite crystals lies in the crystal plane of the tetrahedral base, a determination of which is essential to understanding the structure of the tetrahedral crystal. The intersection of a plane and a rhombohedral corner is a triangle, as shown in Fig. 6. The crystal plane of this triangle can be determined from its three angles. However, the base of the tetrahedral calcite crystal is an isosceles triangle. The crystal plane of the base is thus uniquely determined by the isosceles angle α, labeled in the inset of Fig. 6. The intersection of either the (010) plane or the (012) plane with a (104) rhombohedron is known to result in an isosceles triangle with an angle of about 91 or 78 deg, respectively [12,13]. In a sampling of

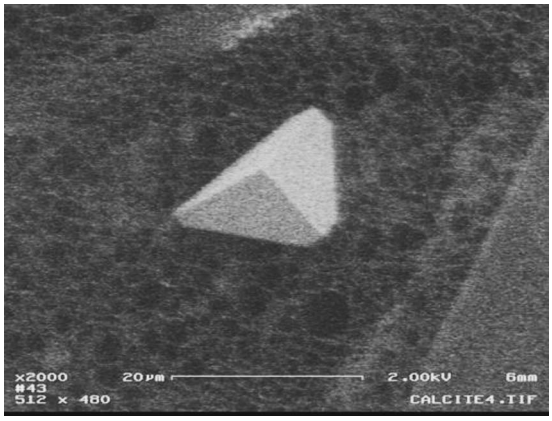

FIG. 5. A scanning electron micrograph of a single tetrahedral crystal oriented base down on a TEM grid. The three basal corners have been cleaved on planes parallel to the upper three faces.

more than 100 tetrahedral *w*-layer crystals from four different samples, over 80% have isosceles triangle bases with the angle α between 75 and 94 deg. This suggests that the bases of the tetrahedral crystals lie on or between the (010) and (012) planes of calcite.

The surface chemistry of the tetrahedral crystals may yield insight into the interactions between them, thus providing an important clue to understanding the ordering of the *w* layer. The (104) plane of calcite is known to have a neutral surface charge, being composed equally of calcium and carbonate ions [12]. However, both the (010) and the (012) faces of calcite are charged homoionic faces composed entirely of either carbonate ions or calcium ions [5,12,13]. For each tetrahedral crystal, the arrangement of a charged (010) or (012) base along with the three neutral (104) faces creates an electric dipole. Furthermore, each crystal is oriented in the same manner with respect to the air-water interface: with its base exposed to the water and its apex exposed to the air.

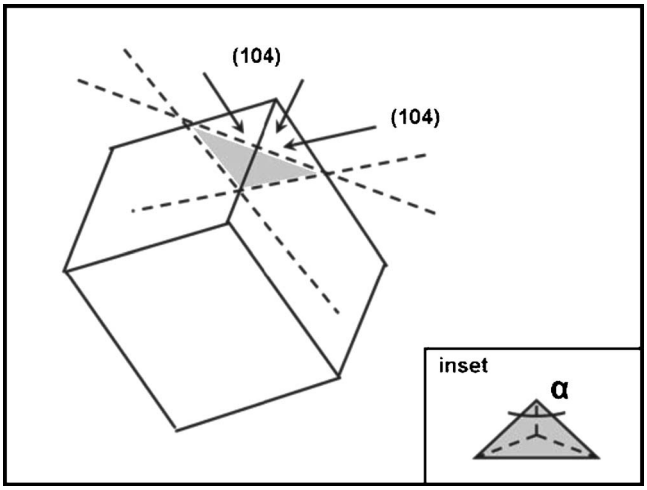

FIG. 6. The intersection of a plane and the corner of a (104) rhombohedral calcite crystal. All arrows indicate (104) crystal planes. The shaded triangle base of the resulting tetrahedron lies on a different plane. The inset shows a view of the tetrahedral crystal from above, with the isosceles angle of the base labeled α.

This orientation would align each electric dipole in the same direction. Furthermore, this orientation is consistent with the proposed surface chemistry, as it would ensure that the charged surfaces are in the water, while leaving the neutral surfaces exposed to the air. Therefore, we hypothesize that the surface chemistry creates an electrostatic dipole-dipole repulsion between each tetrahedral crystal in the *w* layer.

Tetrahedra are not the preferred morphology of calcite crystals; nevertheless they are seen routinely in samples made from heated solutions. To account for this, we propose a mechanism which may form them: convection might initiate more growth of calcite crystals at the interface. Convection may cause ions to rise to the interface at a faster than normal rate, bringing some of the dissolved calcium to the surface of the water even before the calcite precipitates. Calcium carbonate crystals nucleating at the air-water interface may grow into different shapes than crystals grown in the bulk. Crystals growing in the bulk can grow in six isotropic directions into rhombohedra with six (104) faces, while crystals growing at the interface only have three isotropic directions in water and three in air. Perhaps it is this asymmetry in their environments that facilitates the growth of tetrahedral crystals with only three (104) faces. The hypothesis that convection is needed to form the tetrahedral crystals is strengthened by the observation that tetrahedral crystals are seen only rarely in samples made from unheated solutions. The dearth of tetrahedral crystals observed at the bottom of the Petri dish serves as further evidence that tetrahedra nucleate at the interface itself.

In order to compare our experimental observations with our hypothesis for the origin of the ordering of the *w* layer, we assume a functional form for the potential energy interaction between two particles which combines electrostatic repulsion with capillary attraction to create an energetic well occupied by each crystal in the *w* layer. The interparticle potential energy U as a function of distance r is thus given by

$$U(r) = \frac{F^2}{2\pi\gamma}\log\left(\frac{r}{r_0}\right) + \frac{2P^2\epsilon_{air}}{4\pi\epsilon_0 r^3 \epsilon_{water}^2}. \tag{4}$$

The first term in Eq. (4) denotes the capillary attraction, where F is the buoyancy force, γ the interfacial energy and r_0 an arbitrary constant [14]. The buoyancy force is

$$F = \tfrac{4}{3}\pi a^3 g \Delta\rho, \tag{5}$$

where a is the particle radius, $\Delta\rho$ is the density difference between calcite and water, and g is the gravitation constant. The second term in Eq. (4) signifies the dipole-dipole repulsion, where P is the dipole moment and ϵ is the dielectric constant. The electrostatic repulsion is determined by the dipole moment

$$P = a_w^2 \kappa^{-1} \sigma, \tag{6}$$

where a_w is the radius of the wetted area of the crystal, σ is the surface charge density and κ^{-1} the Debye screening length; in our system $\kappa^{-1} = 2.4$ nm.

From the potential function U we derive expressions for both the equilibrium separation and the stiffness of the potential in terms of the system parameters and the buoyancy force F. The equilibrium separation r_{eq} is the distance where the potential is at a minimum.

$$\left(\frac{\partial U}{\partial r}\right)_{r_{eq}} = 0. \tag{7}$$

Substituting U from Eq. (4) into Eq. (7) yields

$$r_{eq} = \left(\frac{3\gamma\epsilon_{air}}{\epsilon_0\epsilon_{water}^2}\right)^{1/3}\left(\frac{\sigma a_w^2\kappa^{-1}}{F}\right)^{2/3}. \tag{8}$$

The stiffness k is given by the curvature of the potential at the equilibrium distance r_{eq},

$$k = \left(\frac{\partial^2 U}{\partial r^2}\right)_{r_{eq}}. \tag{9}$$

Substituting U from Eq. (4) and r_{eq} from Eq. (7) into Eq. (9) yields

$$k = \left(\frac{3F^{10}}{\gamma^5 8\pi^3}\right)^{1/3}\left(\frac{\epsilon_0\epsilon_{water}^2}{a^4\sigma^2\kappa^{-2}\epsilon_{air}}\right)^{2/3}. \tag{10}$$

The expressions for both k and r_{eq} as given in Eqs. (8) and (10) contain only one unknown physical parameter of the system: σ, the surface charge density on the crystal face submerged in the water. The distances between molecules on the various faces of calcite are known [12], but it is not known how many of these charges ionize in the water, nor how many defects exist on the faces of the tetrahedral crystals.

To compare the theory to the experimental data, we quantify the observed particle-particle interaction by measuring r_{eq}, the equilibrium separation between the tetrahedra and k, the stiffness of the interaction. We use IDL software to analyze a series of digital images and particle-tracking techniques to find the particle centers and measure their motion over time [15]. We observe the motion of 16 tetrahedral w-layer crystals over a period of about 5 min. Crystal positions are generally observed to fluctuate around a single point, with some degree of translational motion, as seen in Fig. 7.

We measure the equilibrium separation distance between crystals in the w layer to find the location of the potential energy well. In order to do so we first calculate the pair correlation function $g(r)$. The pair correlation function contains a number of well-defined peaks, as seen in Fig. 8, which is consistent with a finite section of a crystalline sample. The first peak in $g(r)$ corresponds to the position of the nearest neighbors, and is located at an equilibrium separation of about 50 μm or roughly four crystal lengths. Interestingly, the peaks in $g(r)$ are relatively evenly spaced, at 50, 100, 145, and 190 μm. These peaks do not precisely correspond to the peaks of a two-dimensional hexagonal lattice, even though the crystals appear by eye to be hexagonally ordered. This discrepancy may result from the polydispersity in crystal sizes, or perhaps from the effects of the boundary constraining the w layer.

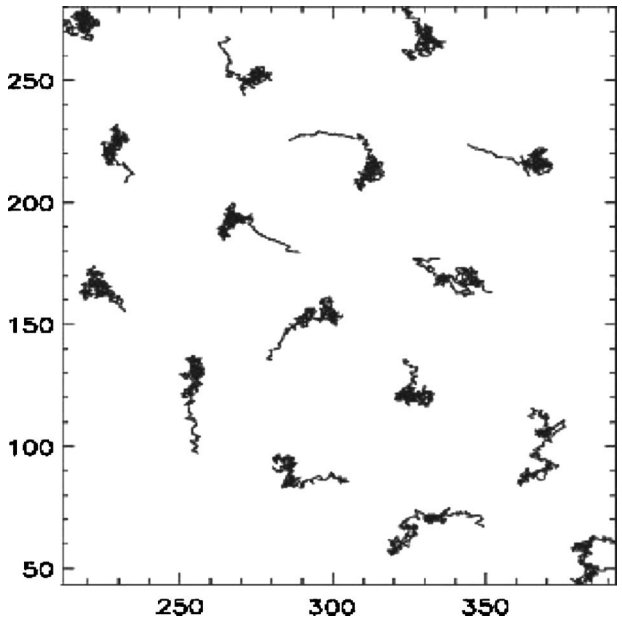

FIG. 7. The x-y trajectories represent the motion of 16 w-layer crystals from Fig. 3 over a period of about 5 min. Each axis is labeled in microns.

We determine the stiffness of the interparticle potential by measuring the position distribution curves for each tetrahedral crystal. The distribution of positions can be understood to be the crystal exploring the potential well. We fit the distribution to a Gaussian profile

$$p(r) = \exp\left(\frac{-r^2}{2\langle r^2\rangle}\right), \tag{11}$$

where $\langle r^2\rangle$ is the variance of position. Assuming sixfold symmetry of the w-layer structure, we can exploit the geometry of the system to invert the Boltzmann distribution and measure $u(r)$ [10]:

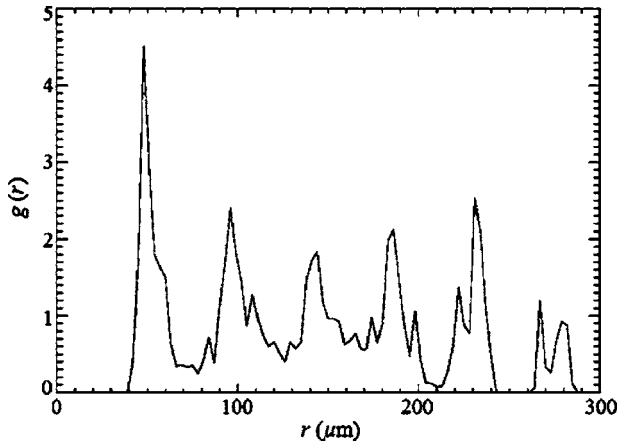

FIG. 8. Pair-correlation function of w layer particles, with a bin size of 3 μm. The equilibrium separation distance is about 50 μm, or four crystal lengths.

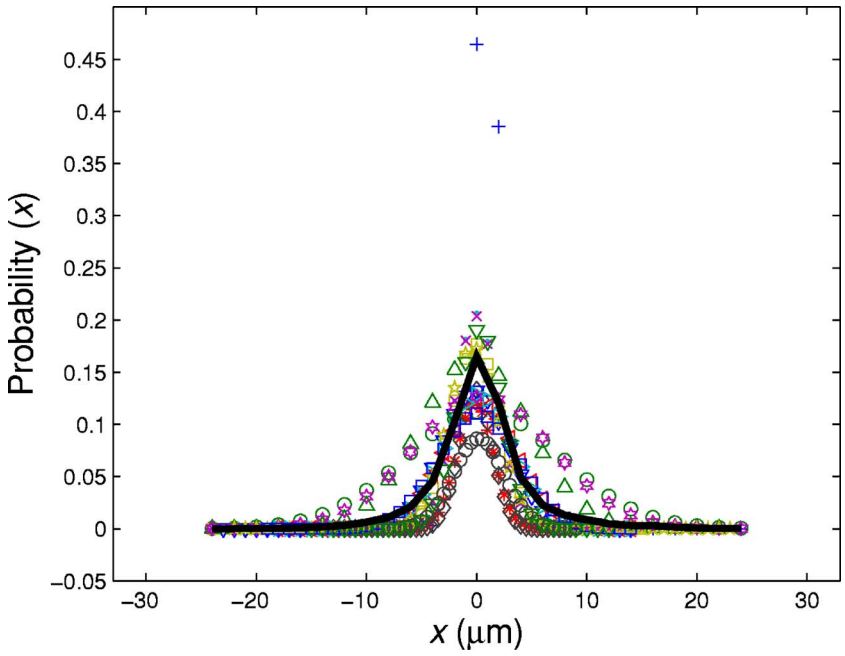

FIG. 9. (Color online) Position histogram of tetrahedral w-layer crystals. Each symbol represents one of 16 different crystals. The solid black line is the average of the data, with a width of 6.34 μm, standard deviation $\langle r^2 \rangle^{1/2} = 2.69$ μm, and stiffness $k = 0.138$ $k_B T/\mu\text{m}^2$.

$$p(r) = \exp\left[\frac{-u(r)}{k_B T}\right]. \tag{12}$$

We approximate the potential near the secondary minimum to be a harmonic potential

$$u(r) = \tfrac{1}{2} k r^2. \tag{13}$$

Equating Eqs. (11) and (12) and with the substitution of Eq. (13) we find the stiffness of the potential to be

$$k = \frac{k_B T}{\langle r^2 \rangle}. \tag{14}$$

By measuring the standard deviation of particle position, we extract measurements of k between 0.02 and 0.45 $k_B T/\mu\text{m}^2$, mostly clustered around 0.14 $k_B T/\mu\text{m}^2$, as shown in Fig. 9.

Comparing the measured values for the equilibrium separation r_{eq} and the stiffness k to the expressions given in Eqs. (8) and (10) we extract a parameter fit for the surface charge density $\sigma = 0.013$ charges/nm^2. By comparison, the maximum surface charge density on the (010) and (012) crystal planes of calcite is on the order of 1 charge/nm^2 [12]. However, we might expect to find one charge per square of the Bjerrum length λ_B, which measures the distance between two charges when their interaction energy is $k_B T$. In water $\lambda_B = 7$ nm, hence we may expect at most one charge per 50 nm^2, or $\sigma = 0.02$ charges/nm^2. Our fit yields a surface charge density that this is a consistent with this value.

In addition, the measurements of the interparticle interaction describe the stability of the w layer. Given the measured values of k and r_{eq}, the depth of the potential well at the equilibrium separation distance is predicted to be on the order of 100 $k_B T$, as seen from Eq. (13). This suggests that the w layer is stable to thermal fluctuations. Changing the solution conditions may disrupt this stability or alter the properties of the w layer. For instance, the model predicts that decreasing the Debye screening length by an order of magnitude would decrease the equilibrium separation by a factor of 5 while increasing the stiffness of the interparticle potential by a factor of 20, as seen through Eqs. (8) and (10). However, this change would not significantly affect the potential well depth at the equilibrium separation distance. This suggests that changes in the molarity of the solution may not affect the stability of the w layer.

The surface charge parameter fit suggests that the functional form chosen for the interaction potential gives an appropriate description of this system. A combination of capillary attraction and dipole-dipole repulsion is sufficient to lead to the ordering of the w layer. The dipole-dipole repulsion arises due to the surface chemistry of the tetrahedral crystals. In fact, even tetrahedral crystals with partially ionized bases will experience the forces required for them to order into a w-layer configuration. The evidence strongly supports our hypothesis that the w layer originates from a combination of capillary attraction and electrostatic repulsion mediated by the surface charging on the crystals themselves.

CONCLUSION

We have shown that tetrahedral calcite crystals, whose growth is facilitated in samples made from heated solution, self-assemble due to a combination of gravitationally induced attractive capillary forces and repulsive dipole-dipole interactions produced by the arrangement of surface charges unique to these tetrahedral calcite crystals. Colloidal ordering and stability are of great significance in a variety of technological, biological, and environmental applications. The ability to obtain a controlled array of micron-sized calcite crystals at the air-water interface may have broad implications in both colloidal and environmental science. Various techniques have been developed to manipulate the growth and arrangement of ordered phases, including those involv-

ing self-assembled monolayers [16] and optical tweezers [17]. However, techniques which exploit the properties of the original colloidal materials themselves may prove to be more versatile. Here we have presented an example of self-assembly where no template is required. Furthermore, calcite is one of the most common sources of scaling impurities in oil and gas production, water purification, and in any environmental or industrial system using large amounts of water [18]. A greater understanding of the behavior of calcite, especially as it precipitates out of a heated solution, might have implications for more effective prevention of calcite scale.

ACKNOWLEDGMENTS

We thank Joanna Aizenberg, Michael Brenner, and Ram Seshadri for insightful discussions, and David Lange, Yuan Lu, and Akobuije Chijioke for help with the SEM measurements. This work was funded by the National Science Foundation (DMR-997142 and DMR-0243715), and by the Harvard MRSEC (DMR-0213805).

[1] T. Nakayama, A. Nakahara, and M. Matsushita, J. Phys. Soc. Jpn. **64**, 1114 (1995).
[2] P. A. Kralchevsky and K. Nagayama, Adv. Colloid Interface Sci. **85**, 145 (2000).
[3] G. Y. Onoda, Phys. Rev. Lett. **55**, 226 (1985).
[4] J. N. Israelachvili, *Intermolecular and Surface Forces*, 2nd ed. (Academic Press, Boston, 1992).
[5] A. Berman, D. J. Ahn, A. Lio, M. Salmeron, A. Reichert, and D. Charych, Science **269**, 515 (1995).
[6] S. Mann, J. M. Didymus, N. P. Sanderson, B. R. Heywood, and E. J. A. Samper, J. Chem. Soc., Faraday Trans. **86**, 1873 (1990).
[7] H. H. Wickman and J. N. Korley, Nature (London) **393**, 445 (1998).
[8] R. Seshadri (personal communication).
[9] Y. Kitano, Bull. Chem. Soc. Jpn. **35**, 1973 (1962).
[10] M. G. Nikolaides, A. R. Bausch, M. F. Hsu, A. D. Dinsmore, M. P. Brenner, C. Gay, and D. A. Weitz, Nature (London) **420**, 299 (2002).
[11] D. Stamou, C. Duschl, and D. Johannsmann, Phys. Rev. E **62**, 5263 (2000).
[12] F. Lippmann, *Sedimentary Carbonate Minerals* (Springer-Verlag, Berlin, 1973).
[13] J. Aizenberg (personal communication).
[14] D. C. Morse and T. A. Witten, Europhys. Lett. **22**, 549 (1993).
[15] J. C. Crocker and D. G. Grier, J. Colloid Interface Sci. **179**, 298 (1996).
[16] A. D. Dinsmore, J. C. Crocker, and A. G. Yodh, Curr. Opin. Colloid Interface Sci. **3**, 5 (1998).
[17] E. R. Dufresne and D. G. Grier, Rev. Sci. Instrum. **69**, 1974 (1998).
[18] S. L. He, A. T. Kan, and M. B. Tomson, Appl. Geochem. **14**, 17 (1999).